

A CRILES-search for H_3^+ emission from the hot Jupiter atmosphere of HD 209458 b[★] (Research Note)

L. F. Lenz¹, A. Reiners¹, A. Seifahrt², and H. U. Käuff³

¹ Institute for Astrophysics, University of Goettingen, Friedrich-Hund-Platz 1, 37077 Goettingen, Germany
e-mail: lealenz@astro.physik.uni-goettingen.de

² Department of Astronomy and Astrophysics, University of Chicago, IL 60637, USA

³ European Southern Observatory (ESO), Karl-Schwarzschild-Str. 2, 85748 Garching, Germany

Received 16 January 2015 / Accepted 11 March 2016

ABSTRACT

Close-in extrasolar giant planets are expected to cool their thermospheres by producing H_3^+ emission in the near-infrared (NIR), but simulations predict H_3^+ emission intensities that differ in the resulting intensity by several orders of magnitude. We want to test the observability of H_3^+ emission with CRILES at the Very Large Telescope (VLT), providing adequate spectral resolution for planetary atmospheric lines in NIR spectra. We search for signatures of planetary H_3^+ emission in the L' band, using spectra of HD 209458 obtained during and after secondary eclipse of its transiting planet HD 209458 b. We searched for H_3^+ emission signatures in spectra containing the combined light of the star and, possibly, the planet. With the information on the ephemeris of the transiting planet, we derive the radial velocities at the time of observation and search for the emission at the expected line positions. We also apply a cross-correlation test to search for planetary signals and use a shift and add technique combining all observed spectra taken after secondary eclipse to calculate an upper emission limit. We do not find signatures of atmospheric H_3^+ emission in the spectra containing the combined light of HD 209458 and its orbiting planet. We calculate the emission limit for the H_3^+ line at 3953.0 nm [$Q(1, 0)$] to be 8.32×10^{18} W and a limit of 5.34×10^{18} W for the line at 3985.5 nm [$Q(3, 0)$]. Comparing our emission limits to the theoretical predictions suggests that we lack 1 to 3 magnitudes of sensitivity to measure H_3^+ emission in our target object. We show that under more favorable weather conditions the data quality can be improved significantly, reaching 5×10^{16} W for star-planet systems that are close to Earth. We estimate that pushing the detection limit down to 10^{15} W will be possible with ground-based observations with future instrumentation, for example, the European Extremely Large Telescope.

Key words. stars: individual: HD 209458 – infrared: stars – planetary systems

1. Introduction

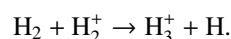
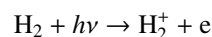
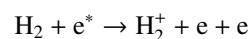
Methods of exoplanet detection have become more and more successful in recent years and various kinds of exoplanets, from hot Jupiters to earth-sized planets, have recently been detected. However, it is still difficult to gain information about the atmospheric composition of these exoplanets. Only a small fraction of the detected exoplanets can be accessed for investigations of the atmosphere, for example, transits and secondary eclipses.

HD 209458 b was the first transiting exoplanet for which an atmosphere was detected in a spectrophotometric observation of Na I (Charbonneau et al. 2002). Most exoplanets with a detection of atmospheric molecules are gas giant planets in close-in orbits. The atmospheres of these extrasolar giant planets (EGP), such as HD 209458 b, are expected to be severely influenced by the stellar extreme ultraviolet (EUV) radiation that drives a hydrodynamic escape in the upper atmosphere. Different models have been derived to estimate the evaporation rate of close-in giant planets (e.g., Lammer et al. 2003).

Some of these models propose that infrared (IR) emissions of H_3^+ ions cool the thermospheres of close-in EGPs and, thus,

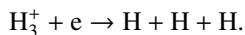
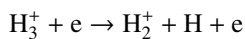
contribute to balance the heating due to the host star radiation (Yelle 2004). H_3^+ emission was detected from the auroral regions of Jupiter by Drossart et al. (1989). The ion was successfully used as a tool to measure atmospheric temperatures and ion densities of Jupiters atmosphere (Yelle 2004). Miller et al. (2000) argue this ion is the main coolant in the ionosphere and thermosphere of Jupiter in both the auroral and nonauroral regions. H_3^+ was also detected in Saturn (Geballe et al. 1993) and Uranus (Trafton et al. 1993). The temperature for the thermosphere of Saturn is measured at around 800 K (Geballe et al. 1993), and for Jupiter a temperature range of approximately 700–1000 K was measured by Lam et al. (1997). Koskinen et al. (2010) measure a mean temperature of 8000–11 000 K for the thermosphere of HD 209458b. H_3^+ is an effective coolant even for high temperatures up to 10 000 K (Neale et al. 1996).

H_3^+ is formed by a reaction of H_2^+ , under EUV radiation and energetic electron precipitation along magnetic field lines, reacting with neutral H_2 , i.e.,



[★] Based on observations collected at the European Organisation for Astronomical Research in the Southern Hemisphere, Chile, 086.C-0045.

The ion is destroyed by the dissociative recombinations



So far H_3^+ emission has not been detected in the atmosphere of an EGP on a planet outside of our solar system. A detection would help to understand the thermal structure of EGPs. Additionally, the planetary radial velocity could be measured directly: since H_3^+ is not formed in stellar atmospheres, a detection could safely be assigned to the exoplanet of the observed stellar system.

The theoretical predictions for H_3^+ emitted from exoplanet atmospheres vary by several magnitudes in the different models. [Miller et al. \(2000\)](#) estimated an emission limit of $\sim 10^{17}$ W for a planet similar to τ Boo b. [Yelle \(2004\)](#) investigated the case of HD 209458 b with a one-dimensional model of an EGP atmosphere. He calculated an emission limit of 1×10^{16} W emitted from the lower thermosphere. At higher altitudes he derived temperatures of 10 000 to 15 000 K, where H^+ becomes dominant and suppresses the formation of H_3^+ .

The lowest estimations for the H_3^+ emission limits of close-in EGPs are derived by [Koskinen et al. \(2007\)](#): With their model of a coupled thermosphere and ionosphere they performed three-dimensional, self-consistent global simulations for different orbital distances of EGPs around a sunlike host star. They conclude, that EGPs are cooled efficiently by H_3^+ inside 0.2–1 AU orbits and state that thermal dissociation and dissociative photoionization of H_2 hampers the emission for orbits closer than 0.1 AU. With their simulation they derived a total power output of $\sim 10^{15}$ W for a hot Jupiter planet in a 0.1 AU orbit and calculated a spectral line output of $\sim 10^{12}$ W for the intensity of the $Q(3, 0)$ -transition.

[Brittain & Rettig \(2002\)](#) reported the detection of H_3^+ emission signals from observations of HD 141569 A. However these observations could not be confirmed by observations made by [Goto et al. \(2005\)](#), who measured upper emission limits that were significantly lower than the signals reported by [Brittain & Rettig \(2002\)](#) while achieving comparable data quality. The most extensive observation attempt for H_3^+ emission from hot Jupiter systems was carried out by [Shkolnik et al. \(2006\)](#). They observed six close-in EGPs with CSHELL at the NASA IRTF. They searched for emission from the $Q(1, 0)$ -transition at 3953.0 nm and calculated emission limits around 1×10^{18} W from their measurements. The lowest limit is reached for GJ 436 with 6.3×10^{17} W. [Laughlin et al. \(2008\)](#) reported an emission limit of 9.0×10^{17} W for observations of τ Boo with CSHELL. [Maillard & Miller \(2011\)](#) suggested an observation strategy using high spectral resolution and possibly occultation spectroscopy in order to differentiate planetary and stellar flux. They stated that the growing sample of known exoplanets also offers more possible candidates for the search for H_3^+ emission.

This work investigates the feasibility of H_3^+ observations with CRIRES ([Kaeufel et al. 2004](#)) at the VLT. The CRIRES spectrograph provides the highest resolution in the IR that is available today.

2. Observations

The observations were carried out with CRIRES ([Kaeufel et al. 2004](#)) at the VLT. The spectra were taken with the reference wavelength set to 4010 nm in the L' band with a resolving power of $R \sim 100\,000$.

Our chosen setting covers seven H_3^+ lines that were found in strong emission in the southern auroral zone of Jupiter by

Table 1. Wavelength coverage of the observed spectra for each of the four CRIRES detectors and the H_3^+ emission line positions and intensities from the southern aurorae of Jupiter as given in [Maillard et al. \(1990\)](#).

Detector	Wavelength range [nm]	Line position [nm]	Intensity [$\frac{\text{W}}{\text{cm}^2 \text{sr}}$]
1	3947.3–3968.6	3953.0	42.8
2	3974.6–3995.1	3985.5 3987.0 3994.6	45.2 23.5 11.5
3	4000.6–4020.3	4012.0 4013.3	19.3 17.3
4	4025.4–4044.3	4043.2	10.2

Table 2. System parameters ([Southworth 2010](#)).

Object	Spectral type	Distance [pc]	M_{Star} [M_{\odot}]	M_{P} [M_{Jup}]	P_{orb} [d]
HD 209458	G0	47.1	1.01	0.685	3.5247

[Maillard et al. \(1990\)](#). Three of the emission lines of the atmosphere of Jupiter were measured with an intensity larger than $20 \text{ Wcm}^{-2}\text{sr}^{-1}$ and another four emission lines with an intensity above $10 \text{ Wcm}^{-2}\text{sr}^{-1}$.

The line positions are listed in Table 1 with the corresponding intensities from [Maillard et al. \(1990\)](#) and the detector number and wavelength coverage of the four CRIRES detectors, on which the lines fall in the observed spectra. The H_3^+ emission line at 3953.0 nm was also used by [Shkolnik et al. \(2006\)](#) in their search for H_3^+ of hot Jupiter atmospheres.

As a result of unfavorable weather conditions, we were able to record only 16 spectra of HD 209458. The stellar and planetary parameters of HD 209458 are summarized in Table 2. Twelve of the observed spectra were taken during secondary eclipse. Hence, planetary emission might be visible in the four remaining spectra available for analysis; these four spectra are hereafter called combined light spectra. The mean signal-to-noise ratio with exposure times of 150 s is ≈ 71 for the 12 eclipse spectra and for the four combined light spectra.

The observations for HD 209458 were carried out in an ABBA-nodding pattern. The data reduction was performed using the CRIRES pipeline recipes (Version 2.1.1) provided by ESO¹. The optimal extraction of the spectra was performed separately for the A and B frames to avoid a degradation of the spectral resolution due to the curvature of the slit. To correct for atmospheric absorption features and solve for the wavelength solution of the spectra, atmospheric modeling was applied, using the LBLRTM² code with the techniques described in [Seifahrt et al. \(2010\)](#). A typical spectrum (black) with its corresponding telluric spectrum from the modeling (blue) is shown in the upper panel of Fig. 1. In the lower panels the observed-computed (O–C) residuals and observed/computed (O/C) results are shown. To correct for telluric absorption features, the observed spectra are divided by the model spectrum (O/C).

In-dispersion stray light from the CRIRES grating causes 1–3% residual flux in the absorption cores of the observed line profiles for regions with fully saturated telluric features ([Lebzelter et al. 2012](#)). For pointlike sources such as stars, this

¹ <http://www.eso.org/sci/software/pipelines/>

² http://rtweb.aer.com/lblrtm_description.html

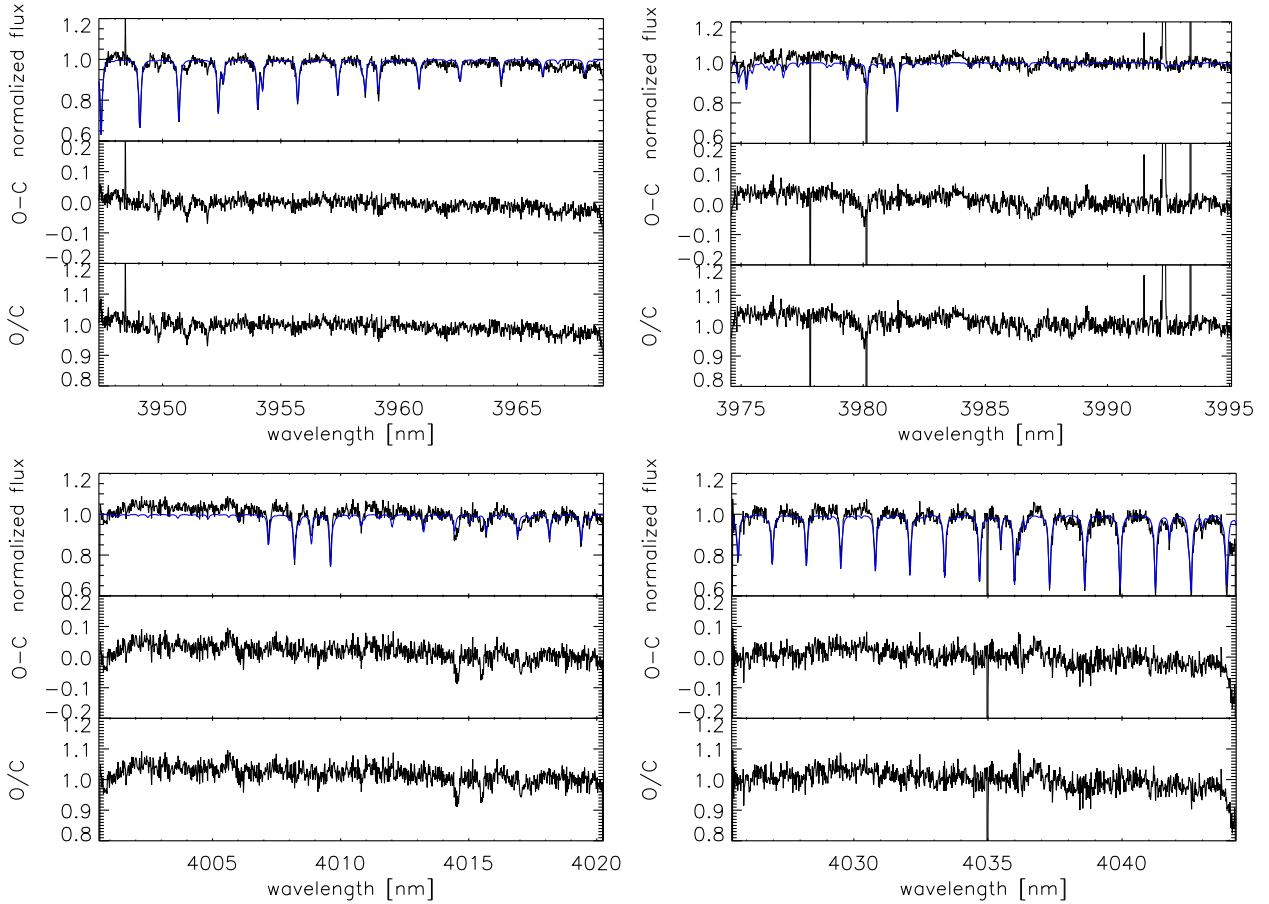


Fig. 1. Example spectrum of HD 209458 for the 4010 nm setting of CRIRES, showing all four detectors. *Upper panel:* CRIRES spectrum (black) and synthetic telluric spectrum (blue) from the telluric modeling. *Lower panels:* observed-computed (O–C) residuals and observed/computed (O/C) results. The O/C spectra are used in the analysis.

effect cannot yet be corrected for. Besides this effect, other systematic deviations caused by the telluric correction with the synthetic model are not expected.

The four detectors have a different continuum level. We assume this trend to originate from the reduction of the flatfields. The spectra were treated with the standard flatfielding recipes for CRIRES provided by ESO.

We use the information on the time of observation, location of the observatory, and the stellar coordinates to calculate the topocentric velocities for the observed spectra and apply the correction to all spectra.

HD 209458 b is a transiting planet and we use the ephemeris value derived by Knutson et al. (2007) to calculate the planetary radial velocity value at the time of each observation. We derive the end of the secondary eclipse from the transit duration given by Beaulieu et al. (2010). Table 3 gives the observation times in MJD format and the calculated radial velocities of the planet for the combined light spectra. Figure 2 shows the radial velocity curve of the orbiting plane. The shaded area indicates the timespan of our observations. The inset shows each separate observation, with the vertical line indicating the end of the secondary eclipse. The uncertainties of the radial velocity resulting from the error of the ephemeris value given by Knutson et al. (2007) are negligible in comparison to the uncertainties of the ephemeris itself. Varying ephemeris values are reported for HD 209458 b and the number of spectra in secondary transit depends on the ephemeris value used. Using, for example, the ephemeris value by Wittenmyer et al. (2005) instead of the

Table 3. MJD and planetary radial velocities of the combined light spectra.

# spectra	MJD	RV planet [km s ⁻¹]
1	55 479.058888248	–32.42
2	55 479.061550962	–33.04
3	55 479.064064636	–33.67
4	55 479.066697450	–34.38

result by Knutson et al. (2007), leads to five spectra where the planet is visible. We choose to use the most recent value derived by Knutson et al. (2007), and its corresponding transit duration from Beaulieu et al. (2010).

3. Search for H₃⁺ emission

3.1. Direct search

We start searching for H₃⁺ emission peaks in each of the combined light spectra separately, considering the radial velocity shift of the planet with respect to its host star. We expect that an emission peak would most probably occur in all combined light spectra, since they were observed within minutes of each other. Since HD 209458 is tidally locked, emission lines from its atmospheres would be very narrow. In the direct search in all

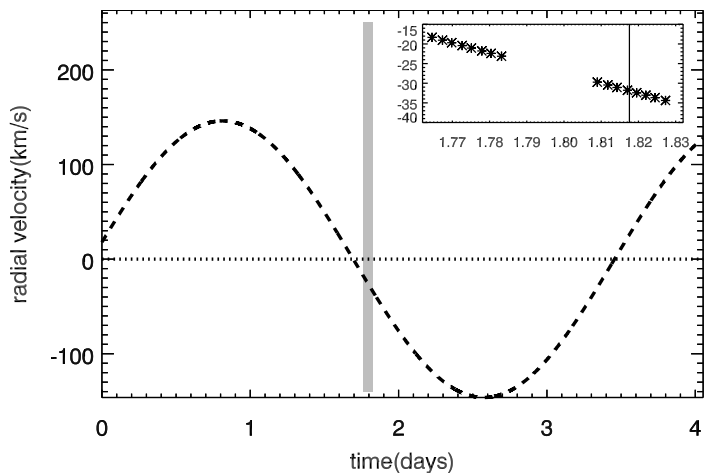


Fig. 2. Radial velocity of HD 209458 b (dashed line). The shaded area indicates the timespan of the observations. The inset shows the different observations with the vertical line indicating the end of the secondary eclipse with the ephemeris value from Knutson et al. (2007) and the corresponding transit duration from Beaulieu et al. (2010). Only observations after this point contain the combined light of the planet and host star.

four combined light spectra, we cannot detect any signatures of H_3^+ emission lines.

3.2. Cross-correlation approach

Our second approach to the search for emission features of the planetary atmosphere is to cross-correlate the combined light spectra pairwise. Emission lines of the planet would show the differential planetary radial velocity in the cross-correlation. Thus, a detection in a cross-correlation would be independent of the accuracy of the knowledge of the H_3^+ emission line positions. The detectors are treated separately because of the gaps between the detectors. Also, a ~ 0.06 nm chunk is cut from both ends of each spectrum to avoid signals from nonlinearity effects at the edges of the spectra. As a preparation for the cross-correlation test, all spectra from detector No. 2 are prepared in the following way: The crack and the right end of the detector is removed. Strong spikes in all spectra are removed and replaced by a median smoothed spectrum.

We apply the cross-correlation to the following combinations of spectra: First, we use the telluric-corrected spectra for the cross-correlation. In the second step, we subtract the host star from the spectra, by computing a mean spectrum of the 12 secondary eclipse spectra and subtract the result from each combined light spectrum before performing the cross-correlations. In the third step, we subtract a single secondary eclipse spectrum instead of the mean eclipse spectrum. This single spectrum has a lower signal-to-noise ratio, but since the timespan between the last observed secondary eclipse spectrum and the combined light spectra is very short, parts of the atmospheric distortions that have not been corrected by the telluric modeling vanish with the subtraction. However, if the ephemeris is not precise one might also subtract a viable signal from the planet. We choose the secondary eclipse spectrum that was observed directly before the end of the secondary eclipse. As a consistency check, we repeat this procedure using the spectrum that was observed second to last during secondary eclipse.

A planetary signal in the spectra is expected to cause a signal in the cross-correlation with the differential planetary radial

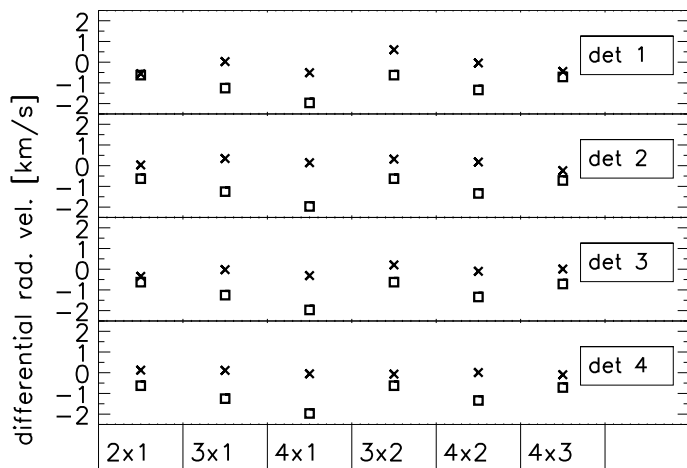


Fig. 3. Cross-correlation results. Upper to lower panels show the four CRIFES detectors. The spectrum that was observed last during secondary eclipse is subtracted from each combined light spectrum. The resulting spectra are cross-correlated and the main peak is fitted with a Gaussian. We derive the radial velocity value from the maximum of the fit and expect a planetary signal to shift the Gaussian fit sideways, producing a signal between 0 km s^{-1} and the differential radial velocity in case of a detection. The squares indicate the calculated differential radial velocity values from the time of observation and ephemeris and the crosses show the measured radial velocity from the cross-correlation. The error bars lie within the symbol size.

velocity of the two spectra that are used as input spectra in the cross-correlation. Since the spectra were recorded in close succession shortly after the secondary eclipse, the differential planetary radial velocity values are only up to 2 km s^{-1} . Also, the stellar and telluric lines, as well as detector artifacts, cause a peak around 0 km s^{-1} .

The cross-correlation results for the pure spectra and the spectra with subtracted mean eclipse spectra show various peaks over the whole radial velocity range. The results for the spectra with subtracted last eclipse spectrum show a clear signal around 0 km s^{-1} as well as the results for the consistency check for which another eclipse spectrum is subtracted before the cross-correlation is applied. We continue the analysis with the spectra from which we subtracted the last spectrum that was observed during secondary eclipse.

We fit the main peak of each cross-correlation with a Gaussian and derive the radial velocity from the maximum of the fit. We expect a planetary signal in the cross-correlation to shift the Gaussian fit sideways. The fitted velocity would thus lie between 0 km s^{-1} and the differential radial velocity in case of a detection. In Fig. 3 the results of the cross-correlation are presented for all four detectors. The x-axis gives the number of spectra used for the cross-correlations (e.g., 1×2 means the cross-correlation of the 1st and 2nd observed combined light spectra). The squares show the differential planetary radial velocities of the pair of spectra and the crosses give the fitted radial velocity values from the cross-correlations. In case of a detection of planetary emission, we expect the radial velocity values of the fit (squares) to follow the pattern of the differential radial velocity values (crosses) in the plot. We expect a planetary signal to occur in all observed spectra, since they were recorded in close succession.

We cannot find cross-correlation signals that follow the expected pattern of the planetary radial velocity. Fitting the cross-correlation results give signals that scatter around 0 km s^{-1} . The same result follows for the consistency test in which another secondary eclipse spectrum is subtracted from the combined

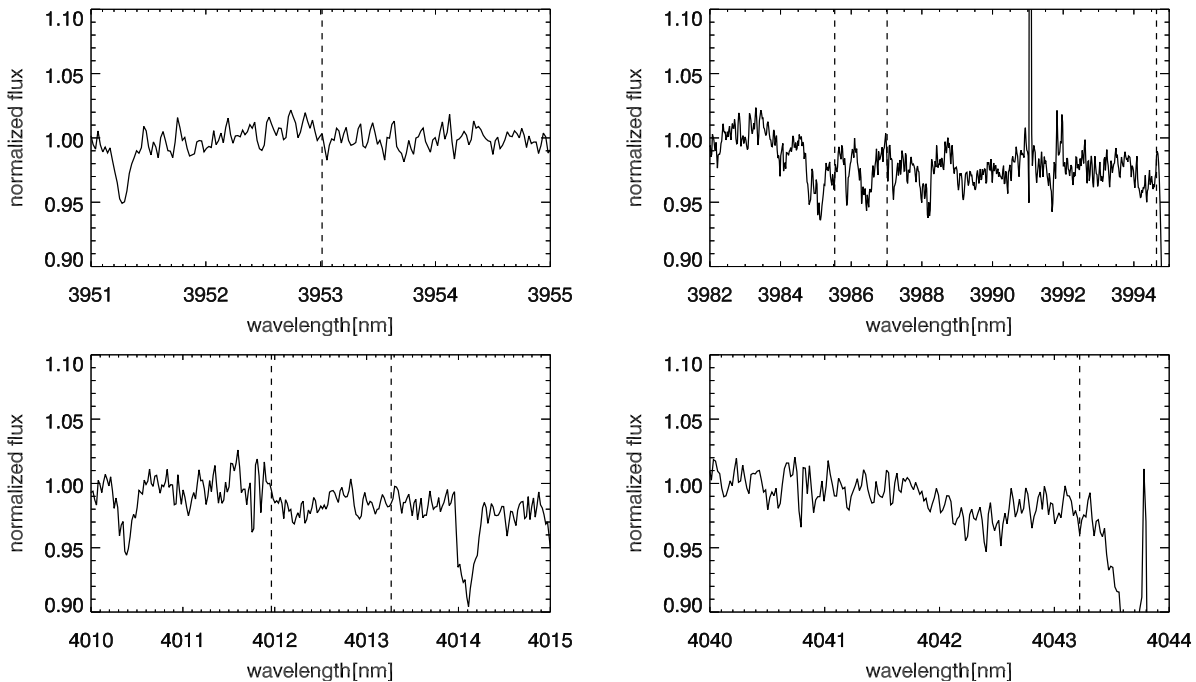


Fig. 4. Spectra of HD 209458, a zoom-in for all four detectors is shown. All observed combined light spectra, were shifted to their apparent radial velocity at the time of observation and then added up binwise. The dashed lines indicate the positions where the H₃⁺ emission lines are expected.

light spectra. We also check all cross-correlation results by eye for peaks and do not detect any signal that indicates planetary emission.

3.3. Search for emission with shift and add

The known ephemeris also enables us to use a shift and add approach to search for H₃⁺ emission: all observed combined light spectra are shifted in wavelength with respect to their apparent radial velocity of the planet at the time of observation. Afterward, the flux is summed up binwise. With this technique the stellar lines and residuals from the telluric correction get blurred and a planetary emission line that is hidden in the stellar flux would emerge in the summation of the shifted spectra, given that the ephemeris and consequent radial velocity values are correct.

The resulting shift and add frame is shown in Fig. 4. The H₃⁺ emission line positions from Maillard et al. (1990) are highlighted by the dashed lines. Insufficient correction of telluric lines by the modeling and the application of the shift and add technique cause artificial, broad absorption lines in the resulting frames. Since we do not apply any correction for the crack on detector No. 2 for this part of the analysis, the crack is still visible as a large peak around 3991 nm in the resulting spectrum. In the results from the shift and add procedure, we cannot detect any signs of emission peaks at the expected H₃⁺ emission line positions.

As a last test for the shift and add results, we create an artificial spectrum; this artificial spectrum contains only Gaussians at the positions of the H₃⁺ line positions from Maillard et al. (1990) and a line width calculated from the thermal width of 0.052 nm folded with the instrumental profile and line strengths of 3σ , which we measure in the resulting shift and add frame at the position of the emission line at 3953.0 nm. We perform a cross-correlation of this artificial spectrum with the resulting shift and add frame as a final test for hidden planetary emission signals

for each detector separately. The cross-correlations do not show a significant peak.

We also search the spectra for a drop of the total flux during secondary eclipse, but cannot identify any variances in the integrated flux that would indicate the end of the secondary eclipse. Variations of the flux due to atmospheric distortions are too large to allow for the measurement of the $\sim 0.1\%$ secondary eclipse depth (Diamond-Lowe et al. 2014).

4. Results

Our search for planetary emission signatures of H₃⁺ in our observed spectra of HD 209458 was not successful. The direct search for the strongest emission lines detected in the aurora of Jupiter by Maillard et al. (1990) shows no emission peaks at the expected line positions. A drawback of this method is that the spectra have to be treated separately, which limits the possible signal-to-noise ratio that could be achieved by combining the observed spectra. Cross-correlating the spectra, after subtracting the last observed eclipse spectrum, gives signals that scatter around 0 km s^{-1} . This method is independent of the knowledge of the precise position of the H₃⁺ lines. A rough estimation of the differential planetary radial velocity would be sufficient to search for the radial velocity shift that would occur in case of a detection. There are weaker H₃⁺ lines measured in the aurora of Jupiter around the strong lines we chose to search for with our direct search (Maillard et al. 1990). These weaker lines could help to detect a planetary signal with the cross-correlation method. The shift and add results show no emission features at the expected line positions. The method could retrieve a signal that was hidden in the stellar signal, since shifting the spectra with respect to the planetary radial velocity blurs the stellar lines. However, it requires the knowledge of the planetary radial velocity and ephemeris to shift the spectra precisely to the planetary radial velocity.

Table 4. Detection limit results.

H ₃ ⁺ line [nm]	Transition	FWHM [nm]	σ	Det. limit [W]
3953.0	Q(1, 0)	0.076	0.0068	8.32 × 10 ¹⁸
3985.5	Q(3, 0)	0.069	0.0072	5.34 × 10 ¹⁸

4.1. Emission limits from the shift and add results

Maillard et al. (1990) find the H₃⁺ emission line at 3985.5 nm, the Q(3, 0)-transition, to be the strongest in their measurements for the auroral zones of Jupiter. Shkolnik et al. (2006) use a different emission line for their search for auroral H₃⁺ emission, the Q(1, 0)-transition at 3953.0 nm. We use our shift and add results to estimate an upper emission limit for planetary H₃⁺ emission from our observations of HD 209458 (Fig. 4) for both H₃⁺ transitions. For the following emission limit calculations, we assume that all planetary H₃⁺ energy is stored in one emission line, following the approach of Shkolnik et al. (2006).

We measure the standard deviation at the positions of the H₃⁺ emission lines at 3985.5 nm and 3953.0 nm in the resulting shift and add spectrum (see Table 4). To estimate the full width at half maximum (FWHM) for the emission lines, we calculate the Doppler broadening of the lines assuming a temperature of 1000 K as a rough estimate for the temperature in the lower thermosphere. H₃⁺ is in strong emission in this temperature range (Miller et al. 2000). We account for the instrumental profile, derived from the measurement of the FWHM of the telluric lines and calculate resulting line widths of $FWHM = 0.76 \text{ \AA}$ for the line at 3953.0 nm and $FWHM = 0.69 \text{ \AA}$ for 3985.5 nm.

To estimate the power output of HD 209458 in the *L'* window, we convert the *K* magnitude, taken from the 2MASS catalog (Cutri et al. 2003) to the *L'* magnitude using the intrinsic colors from Bessell & Brett (1988). We calculate a *L'* magnitude of 6.258. With the *L'* magnitude, the bandwidth (0.65 μm) and flux density for Vega of the *L'* band of $5.267 \times 10^{-11} \text{ W m}^{-2} \mu\text{m}^{-1}$ from Cox (2000), we derive an *L'* band flux for HD 209458 of $1.07 \times 10^{-13} \text{ W m}^{-2}$. Using the distance of $d = 47.1 \text{ pc}$ (see Table 2), we derive the total *L'* luminosity of the star to be $2.85 \times 10^{24} \text{ W}$. This is in good agreement with the bolometric luminosity of HD 209458 by Cody & Sasselov (2002) of $6.1 \times 10^{26} \text{ W}$. For the calculation of the detection limit of our measurements, we assume that a Gaussian of 3σ peak height could be detected and derive the detection limit from the fraction of the total *L'* luminosity in the estimated H₃⁺ equivalent width. We calculate detection limits of $5.34 \times 10^{18} \text{ W}$ for the emission line at 3985.5 nm and $8.32 \times 10^{18} \text{ W}$ at 3953.0 nm.

We compare our results to the theoretical H₃⁺ limits derived by Miller et al. (2000), Yelle (2004), and Koskinen et al. (2007). Miller et al. (2000) used the Jovian ionosphere model (JIM) by Achilleos et al. (1998) and placed Jupiter in a close orbit around the Sun, calculating a total H₃⁺ output of 10^{17} W . Yelle (2004) derived an emission limit of 10^{16} W , based on a one-dimensional model of an EGP while choosing the system parameter to match those of HD 209458 and its orbiting planet. Koskinen et al. (2007) used three-dimensional, self-consistent global simulations of a coupled thermosphere-ionosphere model resulting in a total power output of up to $\sim 10^{15} \text{ W}$. Koskinen et al. (2007) expected the spectral line output for the Q(3, 0)-transition to be 1% of the total output power of H₃⁺, hence a limit of $\sim 10^{12} \text{ W}$. The calculated emission limit for H₃⁺ from the atmosphere of HD 209458 b from our observations is 1 to 3 orders

of magnitude less sensitive than the theoretical predictions. The calculated spectral line output for the emission line at 3953.0 nm by Koskinen et al. (2007) is even 6 orders of magnitude away from our measurements.

Next, we compare our results to the H₃⁺ emission limits reported by Shkolnik et al. (2006) and Laughlin et al. (2008). Shkolnik et al. (2006) measured detection limits for six hot Jupiter systems of different spectral types and reported a detection limit of $6.3 \times 10^{17} \text{ W}$ at 3953.0 nm for the M-dwarf GJ 436 that is one magnitude lower than our measurements. This difference is mainly because of its late spectral type, as the data quality is similar for all spectra used for their analysis. The detection limit results for the late F dwarfs in their sample are comparable to our limit measured for HD 209458 b, a G0 star. Laughlin et al. (2008) reported an H₃⁺ limit for τ-Boo of $9.0 \times 10^{17} \text{ W}$, which is also half a magnitude better than our measurement. Considering the much higher resolution of CRIRES in comparison to CSHELL, but the small amount of observing time for our data, achieving roughly the same order of magnitude for the emission limits seems realistic. Our data was obtained in very short observation time and bad weather. However, even optimal conditions would require significant effort to push the detection limits into the regime of the model predictions as we show in the next section.

4.2. Prospects for future observations

Our upper limits for HD 209458 were achieved in a total integration time of only 600 seconds and with bad weather conditions. There are hot Jupiter hosting stars that are closer to Earth, which increases the detectability of planetary emission. We estimate that for a system at 10 pc distance one could obtain data with sufficient quality to push the detection limit to $5 \times 10^{16} \text{ W}$ in about six hours observation time with CRIRES at the VLT. The data quality would allow us to reach below the theoretical limit given by Miller et al. (2000) and into the regime of the limit given by Yelle (2004) for a few close star-planet systems. Even though CRIRES is the most promising instrument available for this task, it would still not be sufficient to descend to the estimations of Koskinen et al. (2007). The upgrade of CRIRES to CRIRES+ (Oliva et al. 2014), enabling the spectrograph for cross-dispersion, will promote the search for H₃⁺. The continuous spectrum of CRIRES+ will enable the observation of many H₃⁺ emission line positions and thus cross-correlation techniques will be more promising compared to the four separate detectors of CRIRES.

Future telescopes with larger diameters will allow for observations that reach the theoretical predictions of H₃⁺ of exoplanet atmospheres. The European Extremely Large Telescope³ (E-ELT) will have a diameter of 39 m that will dramatically reduce the required exposure times. In Table 5 we compare the exposure times for the observation of H₃⁺ in an exemplary hot Jupiter system. For these estimations we calculate a star-planet-contrast from the theoretical planetary emission limits and use a blackbody for the stellar emission at the H₃⁺ line position at 3953.0 nm. We use the star-planet-contrast to obtain an estimate for the required signal-to-noise ratio for a detection of a planetary signal at this line position. As an exemplary planetary system for the calculation of the observation times, we choose the Gl 86 system, which hosts a $4.01 M_{\text{Jup}}$ planet at 0.11 AU orbital distance (Queloz et al. 2000). The stellar system is only 10.9 pc

³ http://www.eso.org/sci/facilities/eelt/docs/e-elt_constrproposal.pdf

Table 5. Comparison of exposure times for different H₃⁺ emission limits with VLT and E-ELT. We chose Gl 86 as an example candidate system.

Emission limit [W]	Exp. time VLT [min]	Exp. time E-ELT [min]
10 ¹⁷	94	4
5 × 10 ¹⁶	370	16
10 ¹⁶	9300	390
10 ¹⁵	970 000	40 000

away, which increases the possibility of detecting H₃⁺ emission from Earth. Candidate systems for the detection of H₃⁺ emission should preferably be tidally locked, so that the expected emission lines are narrow and very high resolution spectroscopy would enhance the ratio of planetary emission to stellar continuum flux.

We calculate the exposure times for the VLT observations with the CRIRES exposure time calculator⁴ and derive the expected exposure times for the E-ELT assuming a similar performing instrument as CRIRES and accounting for the larger collecting area. Collecting spectra of hot Jupiter systems with a quality sufficient to test the predictions by Miller et al. (2000) and Yelle (2004) will very well be possible. However, reaching the emission limits predicted by Koskinen et al. (2007) for a single emission line of 10¹² W with a ground-based instrument seems unlikely. Evidently, H₃⁺ rotational-vibrational transitions would best be measured from space. MIRI⁵ at James Webb Space Telescope however, does not provide for spectroscopy in this regime. Hence, an instrument such as METIS⁶ on the E-ELT will be of great value (Brandl et al. 2014). As presented right now, METIS Echelle spectroscopy is implemented as a single order integral field mode. For this project a classical cross-dispersed spectrograph such as the updated CRIRES would be preferred.

5. Summary

We carried out an observational test for the detection of H₃⁺ in the atmosphere of a hot Jupiter by analyzing spectra of HD 209458 obtained with CRIRES at the VLT. Our dataset contained 12 spectra taken during secondary eclipse of the transiting planet HD 209458 b and four spectra that contained the combined light of the star and (possibly) the atmosphere of the planet.

We searched for H₃⁺ emission at those line positions that have been found in strong emission in the aurora of Jupiter by Maillard et al. (1990). Our analysis consisted of three different approaches. First, we searched directly for the emission in the observed spectra. Second, we tested a cross-correlation approach, and as a last test, we created a shift and add spectrum by shifting all spectra with respect to their apparent planetary radial velocity at the time of observation and adding up the flux bin-wise. We could not identify any signs of H₃⁺ emission in any of the three steps of the analysis.

From the shift and add results, we calculated an upper emission limit for the two H₃⁺ emission lines that are reported to have the most flux in this wavelength region in the auroral zones of Jupiter. We calculate the emission limit for the line at 3953.0 nm [*Q*(1, 0)] to be 8.32 × 10¹⁸ W and a limit of f 5.34 × 10¹⁸ W for

the emission line at 3985.5 nm [*Q*(3, 0)]. Our emission limits are 1 to 3 orders of magnitudes above theoretical predictions in the literature.

We estimated that data quality sufficient to reach the predicted emission limit of ~10¹⁷ W by Miller et al. (2000) and even a detection limit of 5 × 10¹⁶ W can be achieved with CRIRES for star-planet systems that are close to Earth. However, the faintest H₃⁺ emission limit for a single line flux of ~10¹² W for a close-in hot Jupiter derived by Koskinen et al. (2007) will be difficult to reach with ground-based facilities in the near future. Future giant telescopes, such as the E-ELT will dramatically reduce the required exposure times and thus enable a large sample search for H₃⁺ emission from hot Jupiter atmospheres and may very well push the detection limit down to 10¹⁵ W.

Acknowledgements. We warmly thank Ulf Seemann and Sebastian Schäfer for their help with the data handling and reduction and Johanna Kerch for a thorough reading of the manuscript. Lea Lenz acknowledges financial support from the Deutsche Forschungsgemeinschaft under DFG GrK 1351. Ansgar Reiners has received research funding as a Heisenberg Professor under DFG 1664/9-1.

References

- Achilleos, N., Miller, S., Tennyson, J., et al. 1998, *J. Geophys. Res.*, **103**, 20089
 Beaulieu, J. P., Kipping, D. M., Batista, V., et al. 2010, *MNRAS*, **409**, 963
 Bessell, M. S., & Brett, J. M. 1988, *PASP*, **100**, 1134
 Brandl, B. R., Feldt, M., Glasse, A., et al. 2014, in *SPIE Conf. Ser.*, 9147, 21
 Brittain, S. D., & Rettig, T. W. 2002, *Nature*, **418**, 57
 Charbonneau, D., Brown, T. M., Noyes, R. W., & Gilliland, R. L. 2002, *ApJ*, **568**, 377
 Cody, A. M., & Sasselov, D. D. 2002, *ApJ*, **569**, 451
 Cox, A. N. 2000, *Allen's astrophysical quantities* (Springer)
 Cutri, R. M., Skrutskie, M. F., van Dyk, S., et al. 2003, *VizieR Online Data Catalog: II/246*
 Diamond-Lowe, H., Stevenson, K. B., Bean, J. L., Line, M. R., & Fortney, J. J. 2014, *ApJ*, **796**, 66
 Drossart, P., Maillard, J.-P., Caldwell, J., et al. 1989, *Nature*, **340**, 539
 Geballe, T. R., Jagod, M.-F., & Oka, T. 1993, *ApJ*, **408**, L109
 Goto, M., Geballe, T. R., McCall, B. J., et al. 2005, *ApJ*, **629**, 865
 Kaeufli, H.-U., Ballester, P., Biereichel, P., et al. 2004, in *SPIE Conf. Ser.* 5492, eds. A. F. M. Moorwood, & M. Iye, 1218
 Knutson, H. A., Charbonneau, D., Noyes, R. W., Brown, T. M., & Gilliland, R. L. 2007, *ApJ*, **655**, 564
 Koskinen, T. T., Aylward, A. D., Smith, C. G. A., & Miller, S. 2007, *ApJ*, **661**, 515
 Koskinen, T. T., Yelle, R. V., Lavvas, P., & Lewis, N. K. 2010, *ApJ*, **723**, 116
 Lam, H. A., Achilleos, N., Miller, S., et al. 1997, *Icarus*, **127**, 379
 Lammer, H., Selsis, F., Ribas, I., et al. 2003, *ApJ*, **598**, L121
 Laughlin, L., Troutman, M. R., Brittain, S., & Rettig, T. W. 2008, *BAAS*, **40**, 529
 Lebzelter, T., Seifahrt, A., Utenthaler, S., et al. 2012, *A&A*, **539**, A109
 Maillard, J., & Miller, S. 2011, in *Molecules in the Atmospheres of Extrasolar Planets*, eds. J. P. Beaulieu, S. Dieters, & G. Tinetti, *ASP Conf. Ser.*, 450, 19
 Maillard, J.-P., Drossart, P., Watson, J. K. G., Kim, S. J., & Caldwell, J. 1990, *ApJ*, **363**, L37
 Miller, S., Achilleos, N., Ballester, G. E., et al. 2000, *Roy. Soc. London Phil. Trans. Ser. A*, **358**, 2485
 Neale, L., Miller, S., & Tennyson, J. 1996, *ApJ*, **464**, 516
 Oliva, E., Tozzi, A., Ferruzzi, D., et al. 2014, *Proc. SPIE*, **9147**, 91477R
 Queloz, D., Mayor, M., Weber, L., et al. 2000, *A&A*, **354**, 99
 Seifahrt, A., Käufli, H. U., Zängl, G., et al. 2010, *A&A*, **524**, A11
 Shkolnik, E., Gaidos, E., & Moskovitz, N. 2006, *AJ*, **132**, 1267
 Southworth, J. 2010, *MNRAS*, **408**, 1689
 Trafton, L. M., Geballe, T. R., Miller, S., Tennyson, J., & Ballester, G. E. 1993, *ApJ*, **405**, 761
 Wittenmyer, R. A., Welsh, W. F., Orosz, J. A., et al. 2005, *ApJ*, **632**, 1157
 Yelle, R. V. 2004, *Icarus*, **170**, 167

⁴ <http://www.eso.org/observing/etc/bin/gen/form?INS.NAME=CRIRES+INS.MODE=swspectr>

⁵ <http://www.jwst.nasa.gov/miri.html>

⁶ <http://metis.strw.leidenuniv.nl/>